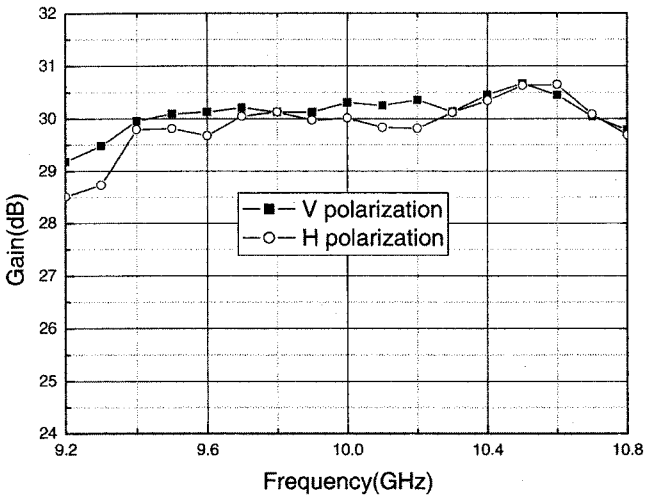

Figure 7 Measured gain vs. frequency for the dual-polarized array

ACKNOWLEDGMENTS

The authors thank X.-J. Shen and W.-T. Huang of ECRIEE for their support of radiation patterns test. The work was supported by the National Natural Science Foundation of China under Grant no. 60402005.

REFERENCES

1. K.R. Carver, Antenna technology requirements for next generation spaceborne SAR systems, In Proceedings of IEEE Antennas Propagation Symposium Houston, TX, June, 1983, pp. 365–368.
2. J. Granholm, K. Woelder, M. Dich, and E. Lintz Charistensen, Dual polarization microstrip antenna array with very low cross-polarization, IEEE Trans Antennas Propag 49 (2001), 1393–1402.
3. S.-C. Gao and S.-S. Zhong, Dual-polarized microstrip antenna array with high isolation fed by coplanar network, Microwave Opt Technol Lett 19 (1998), 214–216.
4. F. Rostan and W. Wiesbeck, Design consideration for dual polarized aperture-coupled microstrip patch antennas, In Proceedings of IEEE International Antennas and Propagation Symposium, 1995, Newport Beach, CA pp. 2086–2089.
5. L.-X. Ling, S.-S. Zhong, and W. Wang, Design of a high isolation dual-polarized slot-coupled microstrip antenna, Microwave Opt Technol Lett 47 (2005), 212–215.
6. S.B. Chakrabarty, M. Khanna, and S.B. Sharma, Wideband planar array antenna in C band for synthetic aperture radar application, Microwave Opt Technol Lett 33 (2002), 52–54.
7. X.-L. Liang, S.-S. Zhong, and W. Wang, Cross-polarization suppression of dual-polarization linear microstrip antenna arrays, Microwave Opt Technol Lett 42 (2004), 448–451.

CORRECTION FACTOR TO BE APPLIED TO THE SAR IN PHANTOM MODELS FOR OCCUPATIONAL ELECTROMAGNETIC EXPOSURE

Wout Joseph, Günter Vermeeren, and Luc Martens
Department of Information Technology, Ghent University/IBBT, Gaston Crommenlaan 8, Box 201, B-9050 Ghent, Belgium

Received 14 July 2006

ABSTRACT: *A correction factor dependent upon frequency, type of phantom, and incident polarization, which should be applied to the measured specific absorption rate is proposed for homogeneous phantoms. It is shown for an application of occupational exposure in the neighborhood of a base station antenna that this correction factor not underestimates realistic exposure of workers.* © 2007 Wiley Periodicals, Inc. Microwave Opt Technol Lett 49: 652–655, 2007; Published online in Wiley InterScience (www.interscience.wiley.com). DOI 10.1002/mop.22249

Key words: *occupational exposure; specific absorption rate; correction factor; base station antenna; electromagnetic radiation*

1. INTRODUCTION

The specific absorption rate (SAR [W/kg]) must be determined and compared to the basic restrictions [1] if one determines the safety distances for occupational electromagnetic exposure of e.g. a GSM base station antenna. In practice, the SAR is experimentally determined in a simple homogeneous phantom, which may result in lower SAR values than the SAR in a heterogeneous and anatomically realistic model [2]. Therefore, the measured SAR must be multiplied by a correction factor [3]. In Ref. 2, a correction factor for E-polarized plane waves was calculated. But to obtain a fully conservative approach (i.e. giving a higher SAR), plane-wave excitation with other polarizations incident on the phantoms under study should be considered, and the SAR values should be compared to those of the realistic model. Three types of polarizations will be considered and a correction factor dependent on the type of polarization, frequency, and phantom is defined. Combining these polarizations (see further) leads to every possible incident field polarization. Therefore, to obtain a fully conservative approach, the highest correction factor for the three investigated polarizations should be considered. This correction factor avoids underestimation of the SAR in contrary to the arbitrary factor 2 defined by CENELEC [3].

2. CONFIGURATION AND METHOD

We investigate electromagnetic plane-wave excitation with different polarizations incident on a homogeneous rectangular box phantom (corresponds to the average trunk of an adult man, CENELEC [3]), a homogeneous prolate spheroid phantom (average man [4], widely used simplified model of a human), and a realistic heterogeneous model of a man (Visible Human, developed at Brooks Air Force Base Laboratories [5]). Plane-wave excitation is a worst-case situation, necessary for the evaluation of safety compliance [2, 3]. For the box and spheroid phantom the dielectric parameters are those of muscle tissues at the investigated frequencies e.g., at 947.5 MHz, a relative permittivity $\varepsilon_r = 54.9$, and a conductivity $\sigma = 0.96$ S/m [3–5]. The density ρ is 1000 kg/m^3. Figure 1 shows the phantoms and their dimensions in front of a base station antenna (see paragraph IV).

Three different polarizations, E (electric field parallel to the major axis of the spheroid or to the longest dimension of other phantoms), H (magnetic field parallel), and K (direction of incidence along the major axis) have been considered. Figure 2 shows the three polarizations incident to the spheroid phantom. For each polarization, the whole-body SAR for the three phantoms has been calculated using finite-difference time-domain (FDTD) simulations [5] and theoretical calculations (one dimensional model for box phantom [2] and formula of Durney [4] for E-polarization for spheroid phantom). Only simulations and theoretical calculations can be used for this investigation because SAR measurements in a heterogeneous model are not possible [1, 3]. We investigate a rather large frequency range of 10–2000 MHz. We define the correction factor Σ for the three polarizations as follows:

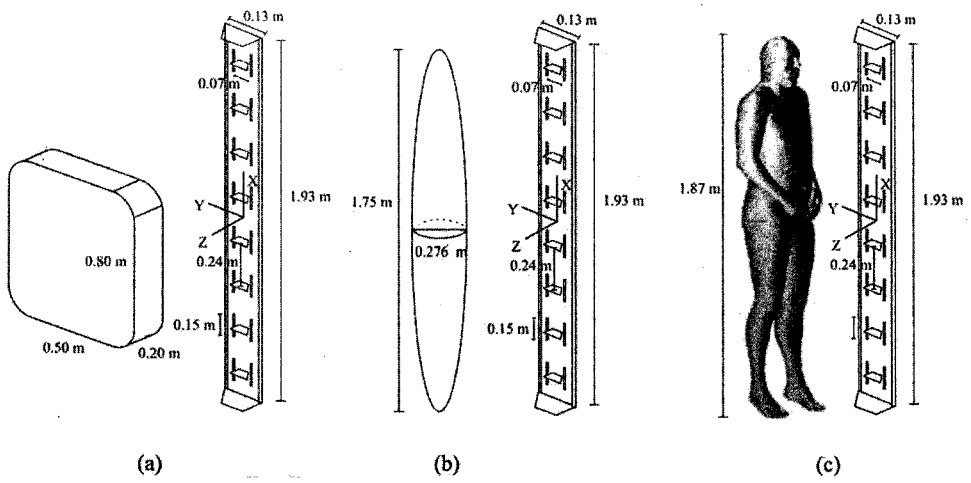

Figure 1 The dimensions of the K736863 GSM antenna and (a) the rectangular box phantom, (b) the prolate spheroid phantom, and (c) the realistic model of a man

$$\sum\Big|^{u}_{\text{phantom}} = \frac{\text{whole} - \text{body SAR}_{\text{human}}}{\text{whole} - \text{body SAR}_{\text{phantom}}}\Bigg|_{u-\text{polarization}} \quad (1)$$

With u = E, H, or K. Thus, Σ depends upon the polarization and is the ratio of the whole-body SAR in the heterogeneous human model and the whole-body SAR in the considered phantom.

To assure a fully conservative approach the maximum value of Σ for the three considered polarizations, noted as $\Sigma^{\max}_{\text{phantom}}$, has to be used. If one combines these three polarizations, every possible incident field polarization can be obtained, and thus using $\Sigma^{\max}_{\text{phantom}}$ avoids underestimation of the SAR. Σ is based on the whole-body SAR, which is the best and most restrictive parameter to take the influence of a phantom into account using plane-wave excitation [1, 2]. By using Σ, the localized SAR will certainly not be underestimated. The advantage of using the safety factor Σ is that for measurements and simulations of the SAR a simple and homogeneous phantom can be used and by applying Σ realistic worst-case SAR values can be obtained.

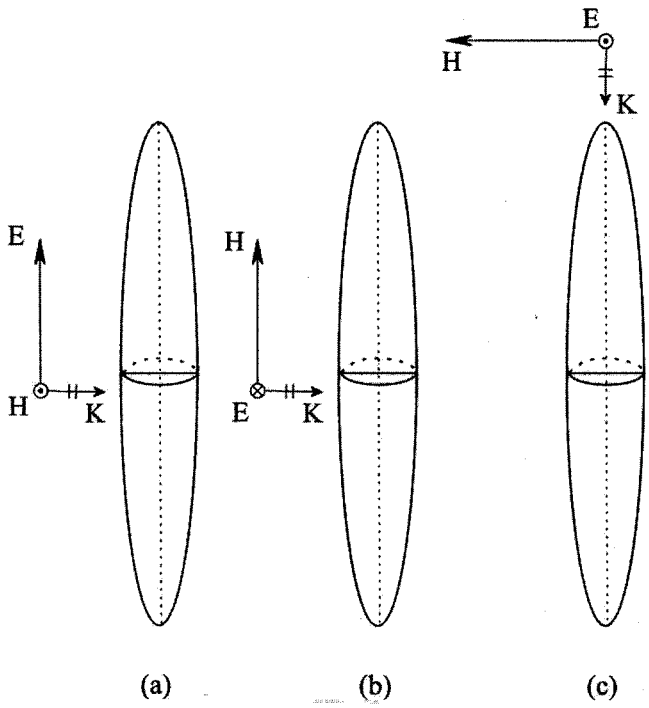

Figure 2 Three different polarizations incident on spheroid phantom: (a) E-polarization, (b) H-polarization, and (c) K-polarization

3. RESULTS

Figures 3 and 4 show Σ for the three polarizations for the rectangular box phantom and the spheroid phantom, respectively. We can clearly see that Σ is frequency- and polarization-dependent. These figures show that Σ for E-polarization has mostly the largest values (e.g., $\Sigma^{\max}_{\text{box}}$ = 2.9 and $\Sigma^{\max}_{\text{spheroid}}$ = 2.5 at 947.5 MHz). For frequencies higher than 500 MHz, Σ varies much less than at lower frequencies. Σ reaches a minimum for the different phantoms and polarizations because of resonance. For E-polarization for example, 73 MHz and 158 MHz are the resonance frequencies of the spheroid phantom and the rectangular box phantom in free space, respectively. The resonance frequency of the realistic heterogeneous model is ~70 MHz for E-polarization, resulting in a local maximum at 70 MHz in Figure 3 [numerator of Eq. (1)].

For the rectangular box phantom, (see Fig. 3) Σ is of the same order for the three polarizations for frequencies higher than 500

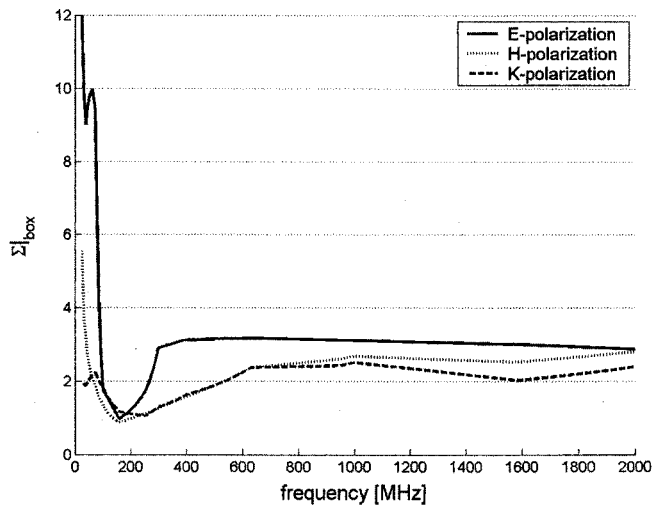

Figure 3 Σ for the rectangular box phantom as a function of the frequency from 10–2000 MHz for the three polarizations under study

MHz, but E-polarization delivers for almost all frequencies the highest correction factor ($\Sigma^{max}_{box} = \Sigma|^{E}_{box}$). For the spheroid phantom (see Fig. 4) Σ is higher for H- and K-polarization than for E-polarization for frequencies lower than 400 and 280 MHz, respectively (e.g., at 100 MHz $\Sigma|^{E}_{spheroid} = 0.6 < \Sigma|^{K}_{spheroid} = 2.4 < \Sigma|^{H}_{spheroid} = 2.6$).

Figure 3 shows that for frequencies higher than 500 MHz, Σ is about 3 (and thus larger than 2 proposed by Ref. 2) for the box phantom. This shows that the arbitrary factor 2 of CENELEC standard 50383 is not a good choice for the rectangular box phantom. We advise to use for each type of phantom the highest value for Σ of the three polarizations at the considered frequency to obtain a conservative approach.

4. APPLICATION IN NEIGHBORHOOD OF BASE STATION ANTENNA

We investigate the SAR in different phantoms in front of a Kathrein 736863 GSM base station antenna (see Fig. 1) using the electromagnetic FDTD simulation tool. The size of the FDTD cell varies from 1 mm to 1 cm. We consider again the rectangular box phantom, the spheroid phantom, and the realistic human model. SAR simulations are performed from 1 mm to 20 cm (occupational exposure) from the antenna. We investigate the K736863 antenna in free space at 947.5 MHz. We used a hard E-field source model applying 1 V/m in the gap of the different dipoles of the base station antenna. Figure 1 shows the dimensions of the model of the antenna together with the rectangular, spheroid phantom, and realistic human model, respectively. The used coordinate system is also shown in these figures.

To show that by applying our correction factor, the SAR in the homogeneous phantoms not underestimates the SAR in the realistic model (in contrary to the application of the arbitrary factor 2 defined by CENELEC [3]), we investigate now the localized SAR averaged over a mass of 10 g [1, 3] because for this configuration, the localized SAR is the most restrictive parameter (not a plane-wave excitation). We define $\Sigma_{10\,g}$ as follows:

$$\sum_{10\,g} = \left.\frac{\text{localized SAR}_{human}}{\text{localized SAR}_{phantom}}\right|_{10\,g} \qquad (2)$$

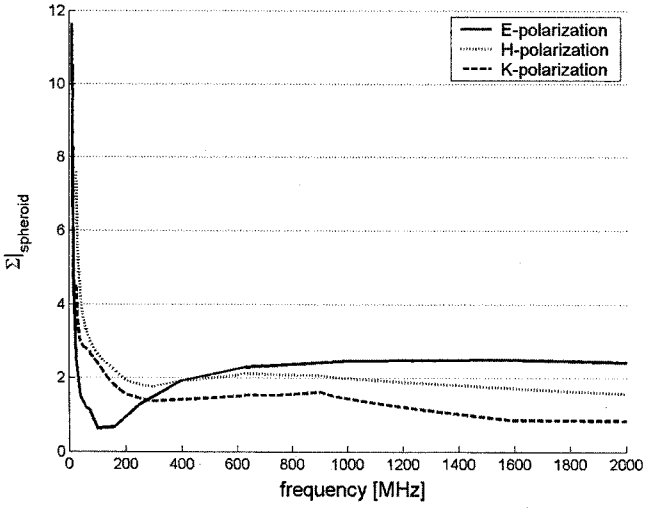

Figure 4 Σ for the spheroid phantom as a function of the frequency from 10–2000 MHz for the three polarizations under study

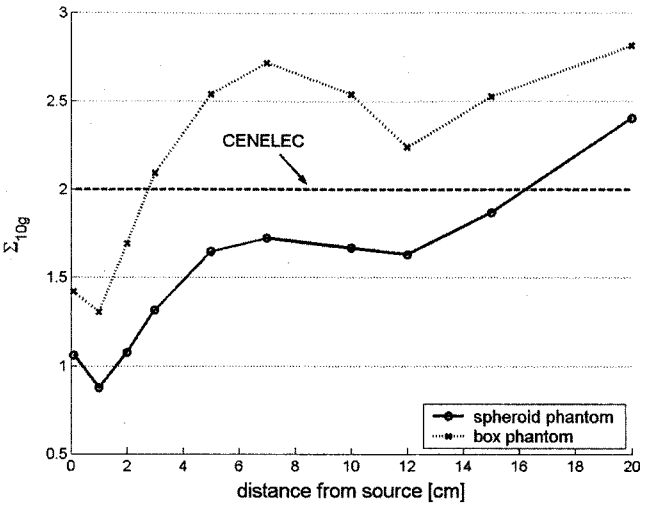

Figure 5 Comparison of $\Sigma_{10\,g}$ for the box phantom, spheroid phantom, and realistic human model in the neighborhood of the K736863 antenna at 947.5 MHz

Instead of using the whole-body SAR in Eq. (1) the localized SAR is used in Eq. (2). Our conservative analysis using the whole-body SAR and plane-wave excitation assures not to underestimate all SAR values, also the localized SAR values. Figure 5 shows $\Sigma_{10\,g}$ for the different phantom models. This figure shows that the arbitrary factor 2 of CENELEC is exceeded for both the rectangular box phantom and the spheroid phantom. This shows again that the arbitrary factor 2 of CENELEC is not a good choice. The spheroid phantom delivers lower Σ values than the rectangular box phantom and is thus more restrictive than the rectangular box phantom. Our correction factor $\Sigma^{max}_{box} = 2.9$ obtained for the rectangular box phantom and $\Sigma^{max}_{spheroid} = 2.5$ for the spheroid phantom at 947.5 MHz is not exceeded (see Section III, Figs. 3 and 4) and thus applicable for this configuration. The realistic human model delivers for most distances the highest localized SAR values ($\Sigma_{10\,g} > 1$), followed by the spheroid phantom and the rectangular box phantom. The curvature of the model has a large influence on the SAR for distances phantom-antenna larger than 2 cm. Also the outer dipoles of the base station antenna (see Fig. 1) then contribute to the maximal localized SAR. For very small distances (1 mm–2 cm), the spheroid phantom is about as restrictive as the human model (at 1 cm even more restrictive, $\Sigma_{10\,g} < 1$ at 1.1 cm). Also the box phantom delivers high SAR values (lower values of $\Sigma_{10\,g}$) for very small distances from the antenna. Very close to the antenna the curvature of the phantom plays a smaller role and mainly the dipoles of the base station antenna, which are located close to the phantom under consideration, contribute to the maximal localized SAR.

5. CONCLUSIONS

A correction factor for the determination of the SAR in a homogeneous phantom exposed in occupational conditions is presented. The correction factor is frequency, phantom, and polarization dependent. To assure a conservative approach, the highest correction factor of the investigated polarizations (E, H, and K) has to be used. An application in the neighborhood of a GSM base station antenna confirms that the arbitrary factor 2 defined in the standard EN50383 of CENELEC is not a good choice.

REFERENCES

1. International Commission on Non-ionizing Radiation Protection, Guidelines for limiting exposure to time-varying electric, magnetic, and electromagnetic fields (up to 300 GHz), Health Phys 74 (1998), 494–522.
2. W. Joseph and L. Martens, Safety factor for the determination of occupational exposure by SAR in phantom model, IEE Electron Lett 39 (2003), 1663–1664.
3. CENELEC EN50383, Basic standard for the calculation and measurement of electromagnetic field strength and SAR related to human exposure from radio base stations and fixed terminal stations for wireless telecommunication systems (110–40 GHz), 2002.
4. H.M.C.H. Durney and M.F. Iksander, Radiofrequency radiation dosimetry handbook, 4th ed., USAF School of Aerospace Medicine, Brooks Air Force Base, 1997. Available at http://www.brooks.af.mil/AFRL/HED/hedr/reports/handbook/contents.
5. J.M. Ziriax, D. Le Blanc, P.A. Mason, and W.D. Hurt, Finite-difference time-domain for personal computers, Proceedings of the 21st Annual Meeting of the Bioelectromagnetics Society, Long Beach, CA, 1999, pp. 57–58.

DESIGN OF MICROWAVE DEVICES BY SEGMENTATION, FINITE ELEMENTS, REDUCED-ORDER MODELS, AND NEURAL NETWORKS

Juan M. Cid,[1] Jesús García,[2] Javier Monge,[2] and Juan Zapata[2]

[1] Departamento de Informática, Universidad de Extremadura, Escuela Politécnica, Campus Universitario s/n, 10071 Cáceres, Spain

[2] Departamento de Electromagnetismo y, Teoría de Circuitos, E.T.S.I. Telecomunicación, Universidad Politécnica de Madrid, Ciudad, Universitaria s/n, 28040 Madrid, Spain

Received 14 July 2006

ABSTRACT: *An accurate and fast neural model for complex microwave circuits is efficiently obtained by using segmentation and exploiting the knowledge of frequency response obtained from reduced order models. Information arriving from the excited modes in the connection ports of the regions to be modeled is included analytically. The frequency response modeling is similar to that of reduced order Padé models, which are used to compute the necessary training data easily. Overall optimization can then be used efficiently. Several examples that illustrate the capacities of the method are also presented.* © 2007 Wiley Periodicals, Inc. Microwave Opt Technol Lett 49: 655–659, 2007; Published online in Wiley InterScience (www.interscience.wiley.com). DOI 10.1002/mop.22248

Key words: *microwave circuit design; segmentation; finite elements; artificial neural networks*

1. INTRODUCTION

Simulation using PCs currently constitutes a very useful and essential tool for designing new devices. Full-wave simulations allow us to compute precise responses of microwave devices, at the expense of increasing computation time and data storage. Design can be seen as an iterative process where the design parameters are updated at each iteration and the device response is then computed. Through the use of overall optimization, it is more certain to achieve design points that fulfill the design specifications, but they always carry out an enormous number of iterations. As many 3D devices usually need and excessive too large computation effort, overall optimization cannot be used efficiently. However, the use of these algorithms can be successfully expanded to more cases by applying artificial neural networks (ANNs) [1, 2].

The main challenge for neural models is the so-called curse of dimensionality, from which it is deduced that the difficulty obtaining the models increases exponentially with the ratio between the number of design parameters and the smoothness of the behavior to be modeled. In an attempt to avoid this handicap, ANNs have been combined with other techniques. In Refs. 3 and 4, the whole device is firstly divided into small regions connected through waveguide segments of arbitrarily shaped sections. Then a neural model is determined separately in each region. The number of design parameters is smaller in each smaller region than in the whole device, and the electromagnetic behavior to be modeled is also smoother. A new method is presented in this work which combines ANNs, segmentation, and the finite element method (FEM) with reduced-order models and already well-known information. The electromagnetic behavior of the regions is described using generalized admittance matrices (GAMs), and this allows us to exploit the frequency dependence of the region's response to achieve a better modeling. Information arriving from modes in the connecting ports is also included analytically.

2. NEURAL NETWORKS

The ANNs more commonly used to model functions are the so-called multi-layer perceptrons (MLPs). Mathematically, an MLP can be described as an application between two real spaces of dimensions D and C, respectively

$$y_k(x,\omega) = \sum_{j=1}^{M} \omega_{kj} \cdot \sigma\left(\sum_{i=1}^{D} \omega_{ji} \cdot x_i + \omega_{j0} \right) + \omega_{k0}, \quad k = 1, \ldots, C \tag{1}$$

where y_k are the coordinates of a point in the output space, x is the position vector of a point in the input space, x_i are the coordinates of this point, ω is a vector whose elements are the weight parameters ω_{kj}, ω_{ji}, ω_{k0} and ω_{j0}, M is the number of hidden neurons, and σ is a sigmoid activation function. It is deduced that an MLP is able to model any continuous multidimensional real function with an arbitrary degree of accuracy by adjusting the weights (training), if the number of hidden neurons is large enough [5, 6].

In modeling a device, the inputs x_i are design parameters sometimes plus frequency. Outputs x_i are parameters that determine the behavior of the device. MLP training starts by computing S samples of the device's true behavior. The number must be large enough to ensure satisfactory training. Next, a cost function is computed that weights the differences between MLP predictions and the training set results. Finally, the weights of the MLP are updated iteratively until a minimum of the cost function is reached. In the examples, weights are updated following a Quasi–Newton algorithm. Derivatives are computed very efficiently by using the back-propagation algorithm.

3. PSEUDO-GENERALIZED ADMITTANCE MATRIX

In Ref. 7, mode-matching and FEM are combined together to compute the GAM of arbitrarily-shaped 3D regions. After several operations the following expression for the GAM is obtained

$$\boldsymbol{Y}(k) = j\frac{k}{\eta_0}\boldsymbol{B}_N^T(k)\,[\boldsymbol{K} - k^2\boldsymbol{M}]^{-1}\boldsymbol{B}_N(k), \quad \eta_0 = \sqrt{\frac{\mu_0}{\epsilon_0}} \tag{2}$$